Combustion Characteristics of H_2/Air Annular Jet Flames using Multiple Shear Coaxial Injectors

Wataru Miyagi[1], Takahiro Miki[1], Tsuneyoshi Matsuoka[2], Susumu Noda[2]

[1]Graduate School of Engineering Toyohashi University of Technology
Toyohashi, Aichi 441-8580, Japan

[2]Department of Mechanical Engineering Toyohashi University of Technology
Toyohashi, Aichi 441-8580, Japan

1 Introduction

The expander bleed cycle (EBC) has been attracting attention for the development of the next-generation rocket engine of Japan because of its simple structure and high safety characteristics. In the EBC, the propellant feed pump is driven by the expanded gas used to cool the combustion chamber. It requires efficient heat absorption to develop a large-thrust EBC, and therefore, predictions about the heat flux and a proper understanding of the effects on the combustion chamber wall are very important [1]. Knowledge about wall heat flux is important for determining the rocket engine life. High-accuracy prediction for the heat flux of the combustion chamber wall is a challenging issue in the development of rocket engines. Furthermore, liquid rocket engines consist of multiple shear coaxial injectors, which enhance the mixing through shear velocity difference. A number of studies have been performed on single nozzle combustion. Daimon et al. (2010) conducted a numerical simulation for H_2/O_2 combustion using a single-element coaxial injector. They reported that the wall heat flux reaches its maximum value at the position where the recirculation vortex attaches to the wall [2]. However, few studies have been conducted for multiple nozzle combustion chambers. This paper presents experimental and numerical studies of the combustion characteristics of H_2/Air annular jet flames and the heat transfer characteristics of the combustion chamber wall when using multiple shear coaxial injectors in a small combustion chamber under normal conditions.

2 Experimental setup and conditions

A schematic of the combustion chamber used in this study is shown in Fig. 1(a). The combustion chamber is made of carbon steel with an inner diameter of 122 mm and a wall thickness of 15 mm, with the length from the injector face to outlet being 480 mm. This chamber was replaced with a Pyrex glass tube when flame pictures were taken. Five shear coaxial injectors are located in the center of the combustion chamber, as shown in Fig. 1(b). One injector is at the center and is surrounded by four other injectors. Figure 1(c) shows a shear coaxial injector consisting of an air post with an inner diameter of 5 mm and an H_2 annulus with an inner diameter of 8 mm. It has a recessed structure with the air injection exit being inset 5 mm from the level of the H_2 injection port to enhance mixing. In this study, we photographed the flames to observe comprehensive flame characteristics of the combustion chamber. In addition, we measured the temperature distribution within the combustion chamber and determined the heat flux through the combustion chamber wall.

The flame pictures were taken with a digital camera (D-90, Nikon). The temperature distributions were measured with an R-type thermocouple of 0.1 mm diameter, which was inserted into the combustion chamber through the outlet. The heat flux was calculated on the basis of the temperature difference between the inner surface of the chamber wall and outer surface temperature using another R-type thermocouple.

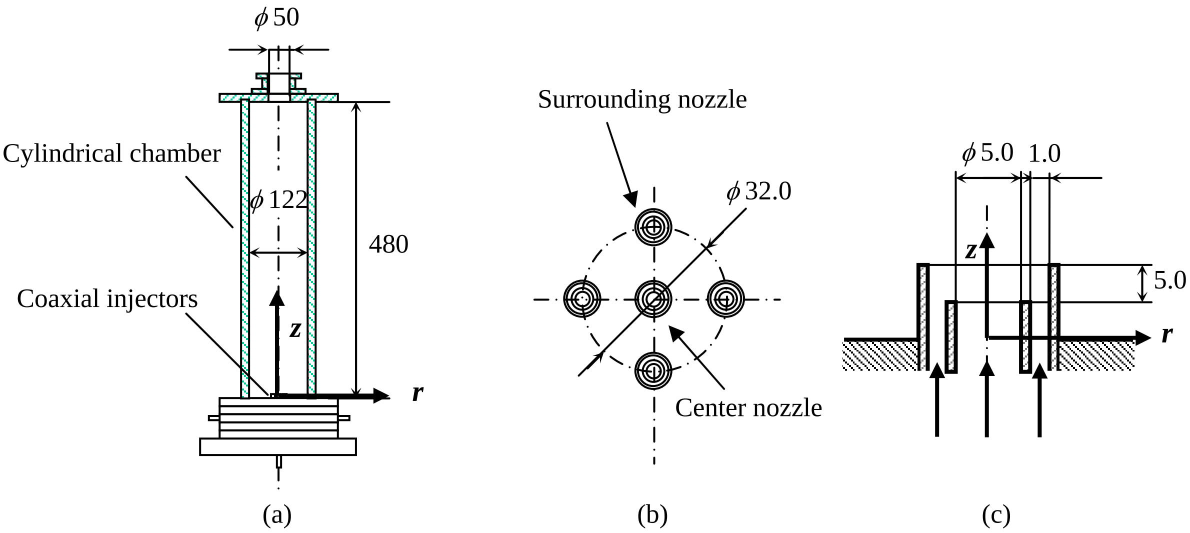

Fig. 1 Schematics of the combustion chamber and coaxial injectors

In this experiment, the oxidizer and fuel were air and hydrogen, respectively. To investigate the influence of turbulence in the combustion chamber, the H_2 and air flow rates were varied from 2.3 Nl/min to 6.0 Nl/min and from 5.6 Nl/min to 14.8 Nl/min, respectively. The overall equivalence ratio ϕ was fixed at 1.0. The Reynolds numbers based on these air flows are Re_{air} = 1500–4000.

3 Simulation method

The governing equations are described below in order of the continuity equation, momentum equation, sensible enthalpy equation, and the conservation equation for mass of species.

$$\frac{\partial\bar{\rho}}{\partial t} + \nabla\cdot(\bar{\rho}\widetilde{\boldsymbol{U}}) = 0\ , \tag{1}$$

$$\frac{\partial\bar{\rho}\widetilde{U}}{\partial t} + \nabla\cdot\left(\bar{\rho}\widetilde{\boldsymbol{U}}\widetilde{\boldsymbol{U}}\right) = -\nabla\bar{p} + \nabla\cdot\left(\mu_l\nabla\widetilde{U}\right) - \bar{\rho}\widetilde{\boldsymbol{U}''\boldsymbol{U}''} + \bar{\rho}g\ , \tag{2}$$

$$\frac{\partial\bar{\rho}\widetilde{h_s}}{\partial t} + \nabla\cdot\left(\bar{\rho}\widetilde{\boldsymbol{U}}\widetilde{h_s}\right) = \nabla\cdot\left(\bar{\rho}\alpha_{eff}\nabla\widetilde{h_s}\right)\ , \tag{3}$$

$$\frac{\partial\bar{\rho}\widetilde{Y_n}}{\partial t} + \nabla\cdot\left(\bar{\rho}\widetilde{\boldsymbol{U}}\widetilde{Y_n}\right) = \nabla\cdot\left(\bar{\rho}D_{eff}\nabla\widetilde{Y_n}\right) + \bar{\dot{\omega}}_n\ , \tag{4}$$

where ρ is the density, $\boldsymbol{U}$ is the velocity vector, p is the pressure, μ_l is the viscosity, g is the gravitational acceleration, h_s is the sensible enthalpy, α_{eff} is the effective thermal diffusivity, D_{eff} is the effective mass diffusivity, Y_n is the mass fraction of species n, and $\dot{\omega}_n$ is the chemical source term of species n. The bar denotes a time-averaged value and the tilde denotes a Favre-averaged value. The standard two-equation k-ε model is employed as the turbulence model. The partially stirred reactor (PaSR) model [3] is employed as the combustion model. Jachimowski's 7-step 7-species kinetic model [4] is employed as the H_2/air reaction model. The simulation code used was reactingFoam from OpenFOAM [5]. The CHEMKIN database was used to calculate the transport coefficients and variables of thermodynamics. The simulation domain corresponds to the experimental equipment shown in Fig. 1, and it is assumed that the periodic boundary condition is applicable for each 90 degrees in the azimuthal direction. The number of cells in the simulation was set to one million, and these cells were refined, especially near the nozzles and flames. The temperatures of the combustion chamber wall obtained from the experiments were used as the boundary conditions for the wall temperature in the simulation.

4 Results and discussion

4.1 Temperature fields

Figure 2 shows the results of both the measurement and simulation of the mean temperature distribution in the chamber for Re_{air} = 3500. The experimental and numerical data appear to be in good agreement with each other. At an axial distance of z = 80 mm, three temperature peaks appear. This shows that each nonpremixed flame front is formed independently at the cross section. The feature disappears downstream of z = 140 mm because of the amalgamation of the flames.

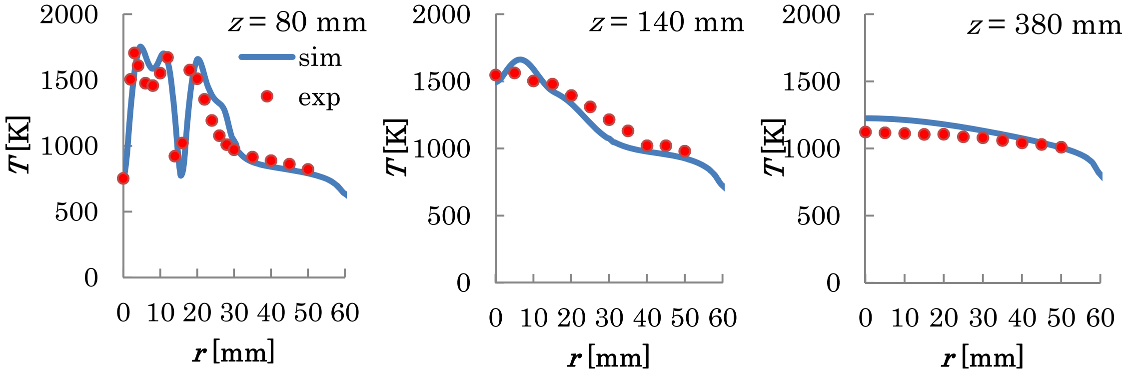

Fig. 2 Radial distribution of mean temperature (Re_{air} = 3500, ϕ = 1.0)

Figure 3 shows a picture of the flames (a) and a numerical mean temperature map (b) for Re_{air} = 3500. In the picture, the blue light-emitting region corresponds approximately to the OH radical emission region, whereas the red light-emitting region is because of the vibrational excitation of water vapor. The distance to the amalgamation of the flames is in good agreement between the experiment and simulation. In the upstream region in Fig. 3(b), each flame appears as an independent flame until flame amalgamation. At the amalgamation point, the temperature increases. Further downstream, the high temperature regions again merge to form a large flame. At this point, the flame becomes squeezed and temperature distribution spreads rapidly in the radial direction downstream. This phenomenon resembles the transition to a turbulent mixture of a jet, even though these flames are in turbulence at the nozzle exit.

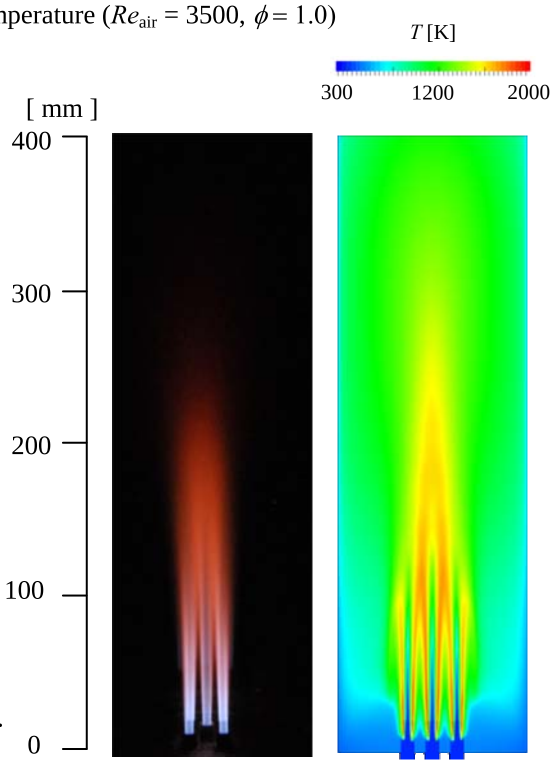

(a) (b)

Fig. 3 Flame photograph and numerical mean temperature map for Re_{air} = 3500

The simulation sufficiently reproduces the features of the flame picture.

4.2 Flow field and heat transfer characteristics

Figure 4 shows the numerical results of the mean axial velocity (a) and the turbulent kinetic energy and experimental results for the heat flux (b) at Re_{air} = 3500. The potential core of the center jet is longer than the cores of the surrounding jets. This may be caused by the suppression of mixing and could be attributable to the decrease in the velocity difference between the center jet and surrounding gases. Another reason could be the mixing of the surrounding jets with the recirculation vortices, as shown in Fig. 4(a). This mixing results in the shortening of the length of their potential cores. The heat flux has a peak between z = 200 mm and 260 mm, which corresponds to the wall attachment position of the recirculation vortex, as shown in Fig. 4(a). Therefore, the location of the recirculation vortex is an important factor that characterizes the wall heat flux distribution. Furthermore, it can be observed from Fig. 4(b) that the curves for the turbulent kinetic energy distribution and heat flux distribution have similar characteristics. Therefore, the flow field also has a strong effect on the wall heat flux.

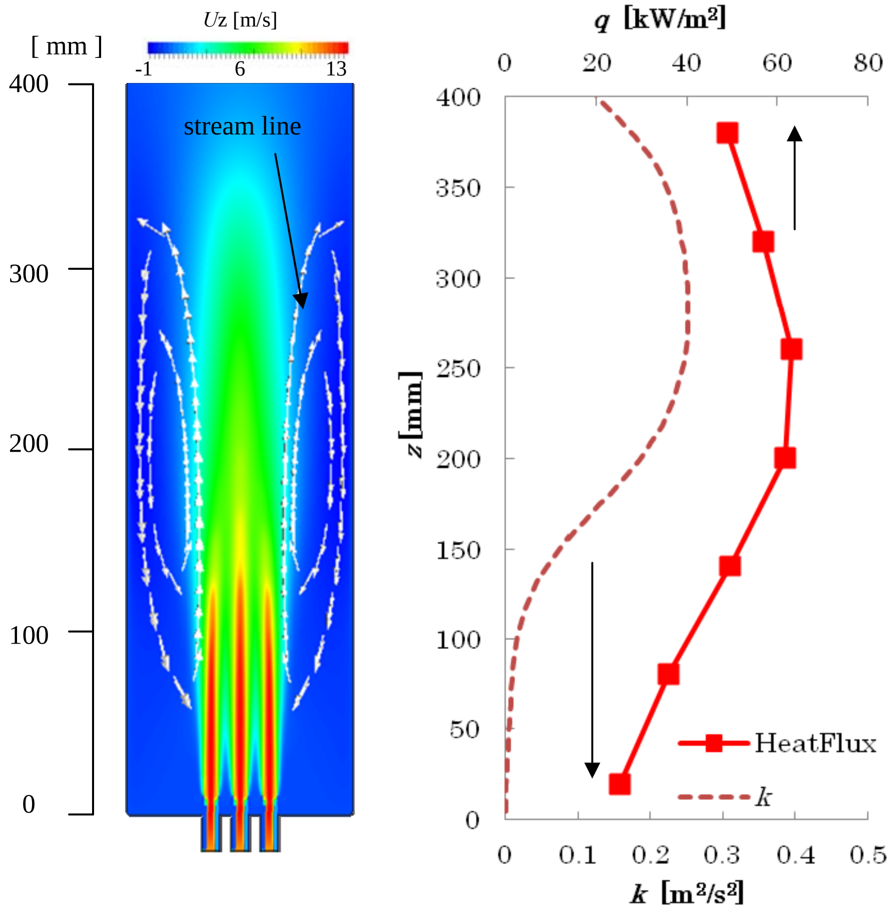

(a) (b)

Fig. 4 Mean axial velocity map (a) and distributions of turbulent kinetic energy and wall heat flux (b) for Re_{air}= 3500

Figure 5(a) shows the mean axial velocity maps with the stream lines of the recirculation zone for Re_{air} = 2500 and 3500. Although the air flow rate was increased, no significant change occurred in terms of the jet width and the size of the recirculation vortex. Figure 5(b) shows the turbulent kinetic energy maps for Re_{air} = 2500 and 3500. In the near field of both cases, the turbulence weakens because of the laminarization phenomenon despite the recessed burner. In the downstream region, the turbulent kinetic energy increases in the shear layer between the jet and surrounding fluid. Therefore, from the above points, it can be concluded that the effect of turbulent heat transport in the near field is small and little heat is transported in the radial direction (Fig. 3). On the other hand, in the downstream region, the heat is strongly transported in the radial direction because of the increase in turbulence. Specifically, the turbulence is generated at the flame amalgamation point. Comparing the two cases, the increase in Re_{air} distributes turbulent kinetic energy widely; thus, the heat is strongly transported in the radial direction.

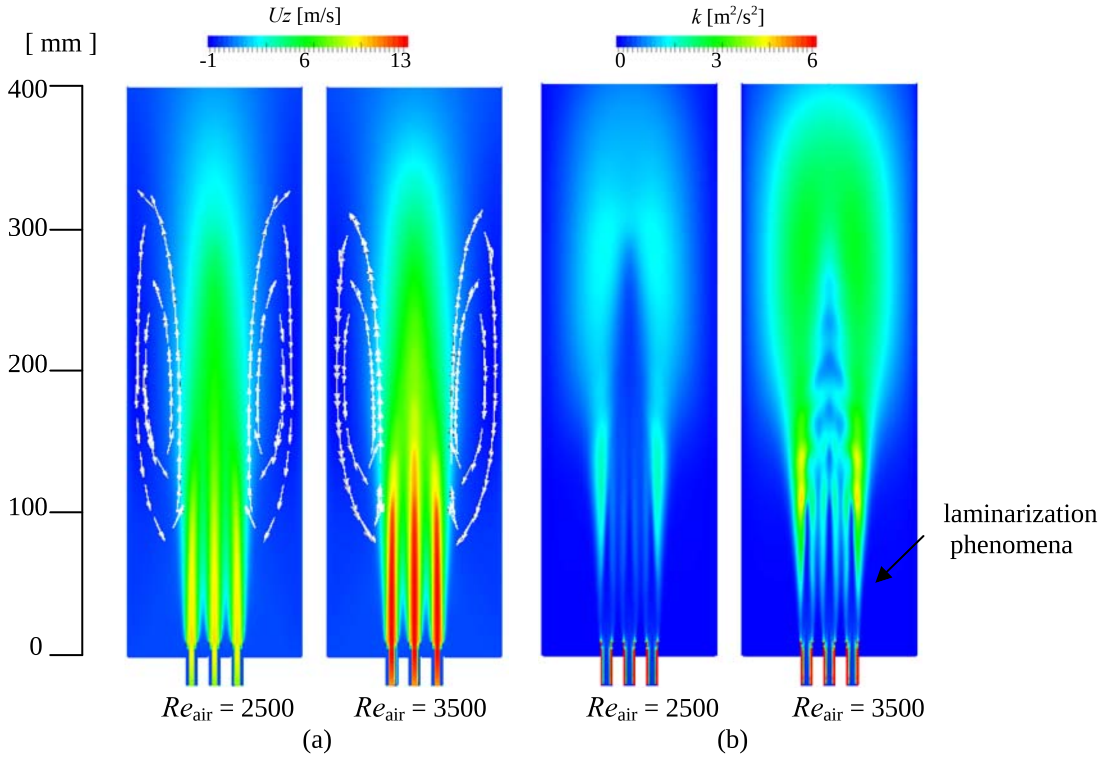

Fig. 5 Mean axial velocity maps (a) and turbulent kinetic energy maps (b)

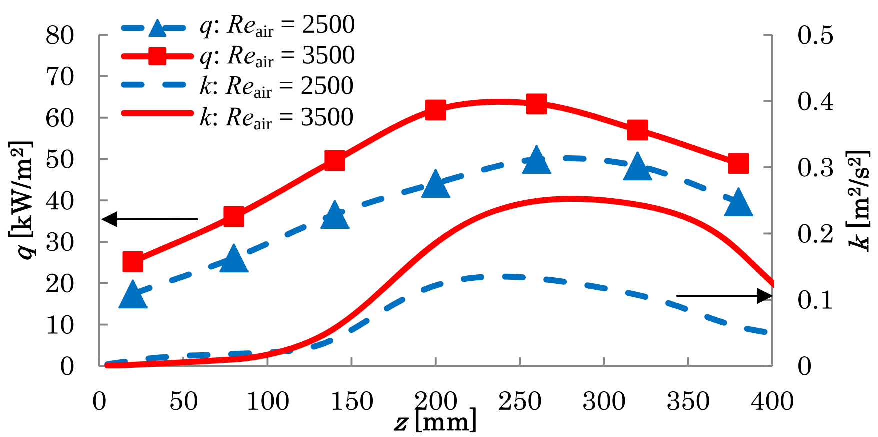

Fig. 6 Distributions of wall heat flux and turbulent kinetic energy

Figure 6 shows the comparison of the wall heat flux and turbulent kinetic energy for Re_{air} = 2500 and 3500. Here the heat flux is experimental and the turbulent kinetic energy is calculated. For Re_{air} = 2500, the wall heat flux gradually increases until z = 260 mm and then decreases in the downstream region. In the case of Re_{air} = 3500, the heat flux also shows a similar trend to that shown for Re_{air} = 2500. However, the peak of the wall heat flux is shifted more upstream. The turbulent kinetic energy increases with Re_{air} and the peak location shifts downstream in contrast to the heat flux. The increase in the turbulence could diffuse the heat generated by the combustion earlier and transport it to the wall.

5 Conclusions

In this study, to understand the combustion and heat transfer characteristics of H_2/air annular jet flames using multiple shear coaxial injectors, we compared the numerical simulation with the experimental results using a small cylindrical combustion chamber and obtained the following conclusions.

(1) Each flame appears as an independent flame until flame amalgamation. At the amalgamation point, the temperature increases. Further downstream, the high temperature regions once again merge and form a large flame. At this point, the flame becomes squeezed and temperature distribution spreads rapidly in the radial direction downstream. This phenomenon resembles the transition to a turbulent mixture of a jet, even though these flames are already in turbulence at the nozzle exit.

(2) The flow characteristics are important for heat transport in the combustion chamber, and the wall heat flux is strongly influenced by it.

(3) In the near field, heat transport is weak because the turbulence is suppressed due to the laminarization phenomenon, despite the recessed nature of the burner. The turbulent heat transport downstream is dominant where turbulence is developed, and thus, the wall heat flux is increased.

(4) Under these conditions, an increase in Re_{air} does not change the size of the recirculation vortex in the combustion chamber, despite the increase in the turbulence’s kinetic energy. As a result, the peak position of the wall heat flux is shifted upstream because the turbulent heat transport is enhanced.

References

[1] Atsumi M, Yoshikawa K, Ogawa A, Onga T. (2011). Development of the LE-X Engine. Mitsubishi Heavy Industries Technical Review. 48:36-41

[2] Daimon Y, Negishi H, Yamanishi N. (2010). Combustion and Heat Transfer Modeling in Regeneratively Cooled Thrust Chambers. AIAA:6723

[3] Golovitchev V.I. (2001). TFR Research Proposal Chalmers University of Tech.

[4] Jachimowski C.J. (1988). An Analytic Study of the Hydrogen-Air Reaction Mechanism with Application to Scramjet Combustion. NASA TP:2791.

[5] OpenFOAM, http://www.openfoam.com/